Stratified Tidal Flow over a Bump

RICHARD DEWEY

School of Earth and Ocean Sciences, University of Victoria, Victoria, British Columbia, Canada

DAVID RICHMOND AND CHRIS GARRETT

Department of Physics and Astronomy, University of Victoria, Victoria, British Columbia, Canada

(Manuscript received 8 October 2004, in final form 22 April 2005)

ABSTRACT

The interaction of a stratified flow with an isolated topographic feature can introduce numerous disturbances into the flow, including turbulent wakes, internal waves, and eddies. Measurements made near a "bump" east of Race Rocks, Vancouver Island, reveal a wide range of phenomena associated with the variable flow speeds and directions introduced by the local tides. Upstream and downstream flows were observed by placing two acoustic Doppler current profilers (ADCPs) on one flank of the bump. Simultaneous shipboard ADCP surveys corroborated some of the more striking features. Froude number conditions varied from subcritical to supercritical as the tidal velocities varied from 0.2 to 1.5 m s^{-1}. During the strong ebb, when the moored ADCPs were located on the lee side, a persistent full-water-depth lee wave was detected in one of the moored ADCPs and the shipboard ADCP. However, the placement of the moorings would suggest that, by the time it appears in the moored ADCP beams, the lee wave has been swept downstream or has separated from the bump. Raw ADCP beam velocities suggest enhanced turbulence during various phases of the tide. Many of the three-dimensional flow characteristics are in good agreement with laboratory studies, and some characteristics, such as shear in the bottom boundary layer, are not.

1. Introduction

This paper will examine measurements made using acoustic Doppler current profilers (ADCPs) in a tidal flow as it interacts with a three-dimensional obstacle. When flows encounter topographic or bathymetric features, they can be disturbed in complex ways. For relatively small features, the effects may be subtle and local. For large features, blocking and wake effects can dramatically alter the flow patterns and influence the large-scale dynamics, through increased drag, for example. If the fluid is stratified, then additional complexities are introduced within the interior of the fluid. Form drag can be partitioned into both barotropic and baroclinic components, tilted isopycnals and wake eddies may cause upwelling or downwelling, turbulent boundary layers and shear instabilities will act to mix and modify the density structure, and internal waves may radiate away, communicating the disturbance to remote areas. The data presented here, although limited, capture some of these complex interactions.

In the ocean, except for the abyssal plains, significant bathymetric features are ubiquitous and can be identified at rocky coastlines, the continental shelf break, along the continental slope in the form of canyons and ridges, at isolated seamounts and volcanoes, and wherever faults and spreading margins give rise to underwater mountain ranges. Although early beliefs suggested that deep ocean currents were weak, recent measurements show that near bottom currents may be both strong and common, and that global tides and large-scale ocean currents may interact significantly with rough bathymetry, causing both local mixing and the generation of internal waves.

Studies of flow past two-dimensional bathymetric changes (shelf breaks and sills) are common (e.g., Cummins et al. 2003) and provide a reasonable framework for an initial understanding of how stratified flows respond to abrupt topography. However, despite their

Corresponding author address: Richard K. Dewey, SEOS, University of Victoria, P.O. Box 3055, Victoria, BC V8W 3P6, Canada.
E-mail: rdewey@uvic.ca

potential interest, few oceanic measurements have been made describing the structure of stratified flows over and around three-dimensional objects. Island wakes were studied by Wolanski et al. (1996), turbulence near seamounts was studied by Lueck and Mudge (1997) and Kunze and Toole (1997), variable depth sills were studied by Klymak and Gregg (2001), a shallow continental shelf bank was studied by Nash and Moum (2001), sidewall ridges were studied by Edwards et al. (2004), the interactions of large-scale tides with a deep ridge were studied by Althaus et al. (2003), and mid-ocean tides with an island chain were studied by the Hawaii Ocean Mixing Experiment group (Rudnick et al. 2003). Atmospheric studies are more numerous, with a recent review by Belcher and Hunt (1998). Baines (1995) is a comprehensive reference for the fluid mechanics of topographic effects in stratified flows. For three-dimensional objects, he draws heavily on the work of Smith (1978, 1980, 1989). Laboratory work has provided some of the more complete realizations (e.g., Hunt and Snyder 1980; Vosper et al. 1999). Modeling studies are also numerous, with considerations of both isolated features (Hanazaki 1994) and 2D sills (Lamb 1994). In many coastal areas, the dynamical effects of topography are further complicated by flow variations associated with the tides, which ebb and flow across the bottom.

2. The setting

Near Race Rocks, at the southern tip of Vancouver Island, British Columbia, there is an isolated "bump" that rises some 70 m in 100 m of water (center of insert, Fig. 1). It is reasonably symmetric, with a half-height radius of approximately 400 m. The sides are steep, with a slope of about 0.15, and the currents are dominated by a mixed-semidiurnal tide with peak speeds that reach 1.5 m s^{-1}. In general, the flood tide flows around Race Rocks (to the west) from west to east, turning toward the northeast over the bump. Ebb tides approach the bump from the northeast, with relatively flat bathymetry over the preceding 5 km. Despite the vigorous tidal mixing, the water column has a relatively strong and uniform stratification with $N \approx 1.1 \times 10^{-2}$ s^{-1} maintained by a sheared estuarine circulation. In June of 2002, we undertook a study of the stratified tidal flow in the vicinity of the bump, with an emphasis on the wake zone during ebb flows. During flood tides, the bump is within the far reaches of the disturbances stretching behind Race Rocks so that it is difficult to isolate the effects of the bump itself.

Parameter space

When a stratified flow interacts with a topographic feature, numerous effects may occur. In a tidal flow, the hydrodynamic conditions may trace out a region of parameter space. The nondimensional parameters for investigation include

$$\frac{U}{Nh}, \quad \frac{h}{H}, \quad \frac{h}{L}, \quad \frac{\omega L}{U}, \quad \text{and} \quad \frac{fL}{U}, \tag{1}$$

where U is the approaching upstream velocity (ignoring any vertical structure for now), N is the buoyancy frequency given by $N^2 = -g/\rho(\partial\rho/\partial z)$ (ditto), h is the height of the bump, H is the water depth, L is the half-width or radius, ω is the frequency of variation of the currents (tides), and f is the local Coriolis frequency (Fig. 2). The most important parameter is likely to be the dimensionless topographic Froude number (Hunt and Snyder 1980),

$$F = \frac{U}{Nh}. \tag{2}$$

Here F, which includes the fixed height of the obstacle, is different from the more classically defined Froude number, which is a ratio of current to wave speed. For low F, conditions associated with strong stratification, tall obstacles, and/or weak flows, the disturbances will be fairly two dimensional and restricted to the horizontal plane. As F increases toward 1, vertical motion becomes more prominent, and the propagation characteristics of internal waves in the flow will influence the response. At large F, the flow may exhibit three-dimensional wakes and be more turbulent. Flow separation may occur at any value of F. Boundary layer and wake effects will also vary in scale, intensity, and location over the expected range of F. Considering the height of our bump (h = 70 m) and observed mean stratification, to a good approximation $F = U(t)/0.77$ (for U in meters per second), such that ebb currents in the range of 0.25–1.5 m s^{-1} will result in topographic Froude numbers between 0.33 and 1.95. Vosper et al. (1999) would suggest that lee-wave-generating near-critical flow conditions occur for $0.6 < F < 0.8$. As the tidal currents trace out ellipses, the current and therefore topographic Froude number never fall entirely to zero.

The scaled height h/H is not likely to be very important until close to 1. Most investigations (Hunt and Snyder 1980; Baines 1995; Nash and Moum 2001) consider deep fluids with $h/H \ll 1$. As h/H approaches 1, the free surface will come into play, and disturbances will be confined vertically. Islands have effectively $h/H > 1$; wake structures may then depend on the island width L and wakes generated on either side of an island may

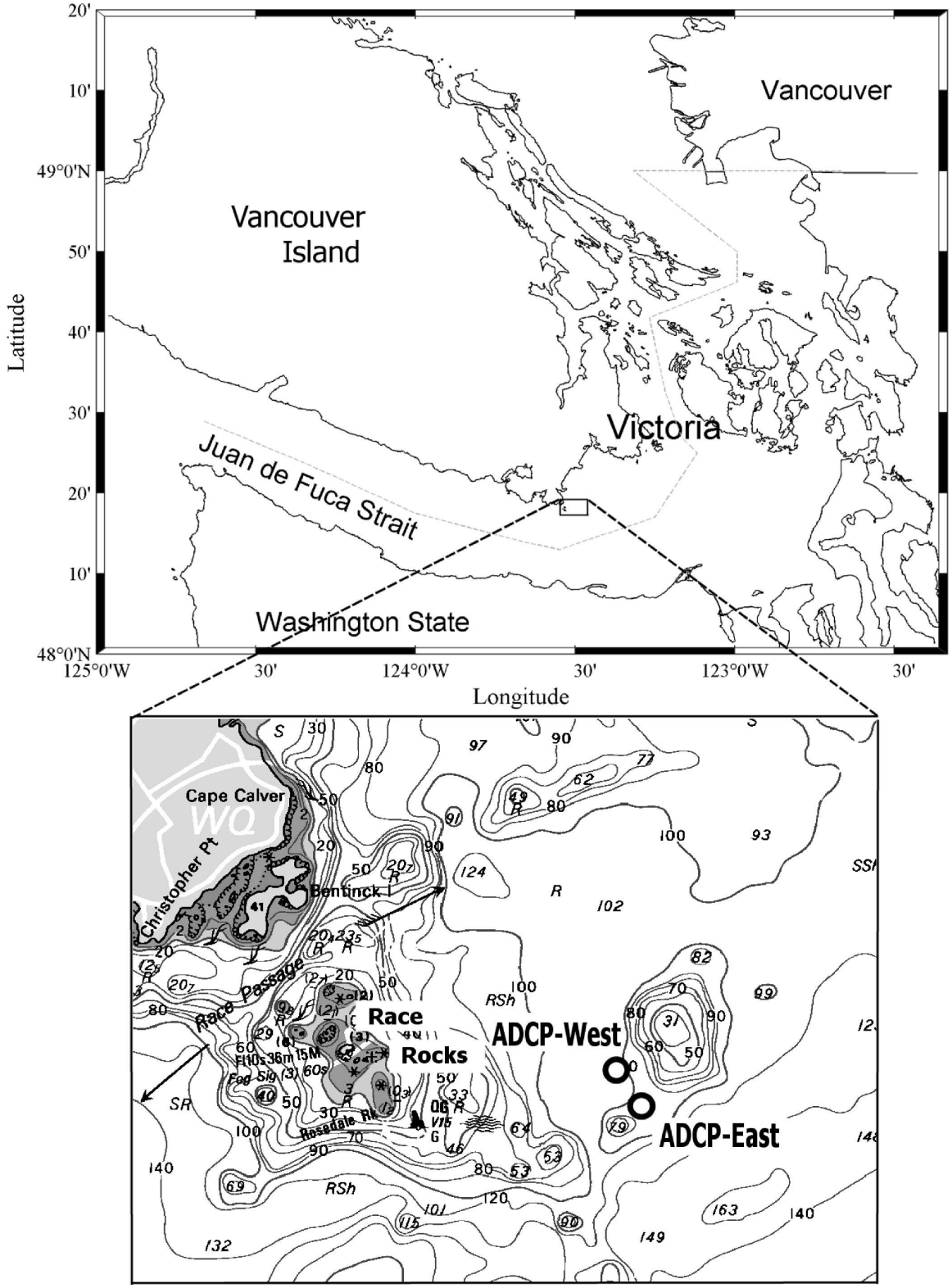

FIG. 1. Our bump is just east of Race Rocks, the southern-most rocky point of Vancouver Island. It is located right of center in the lower chart, rising 70 m above the local flat bottom with a depth of about 100 m. Two bottom-mounted 300-kHz ADCPs were deployed on the ebb-tide lee flanks from 19 to 23 Jun 2002.

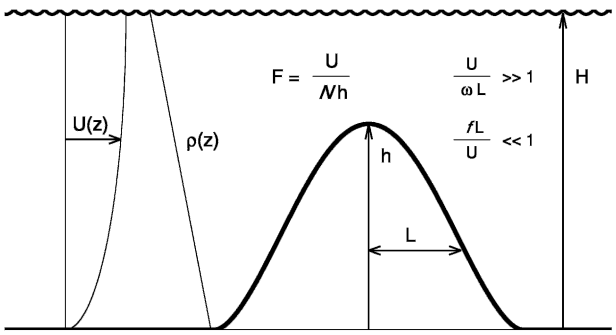

FIG. 2. The interaction of a stratified flow and a bump is characterized by the impinging sheared flow $U(z)$, the stratification $\rho(z)$, the height h and radius L of the bump, water depth H, and possibly rotation f and the rate of change of the flow ω.

interact, as in a vortex street (Wolanski et al. 1996). In our case, h/H is approximately 0.7, and we may expect little influence of the free surface. Wind (deep water) waves, however, are altered by the accelerated flows over the bump. The topographic slope h/L can affect internal wave growth (low h/L) or flow separation (high h/L).

For an oscillating or time-varying flow, the ratio of the obstacle size to the excursion scale $\omega L/U$ is an important parameter. If $\omega L/U \gg 1$, the bump acts as a wavemaker, generating internal waves of frequency ω (e.g., St. Laurent and Garrett 2002). If $\omega L/U \ll 1$, as in our case, the interaction will be quasi steady and significant flow disturbances, such as lee waves, can be expected to grow and develop. However, to release an internal bore or wave train during each tidal cycle, the flow must change slowly with time. For both atmospheric and oceanic flows, the effects of planetary rotation (f) may become important for large, slow interactions for which $fL/U \gg 1$. For relatively fast flows and small obstacles (our bump), rotation is not likely to be important.

3. Expectations

For our bump, for which the topographic Froude number is likely to be the most important nondimensional parameter, we may draw heavily on the laboratory studies of Hunt and Snyder (1980) and sketch out the possible types of flow structures we might expect. At low F ($\approx$0.2), one would expect little flow alteration above the top of the bump, and the approaching fluid below the crest is forced to diverge horizontally around the obstacle. In the wake, vortical modes or even alternating eddies may dominate (Vosper et al. 1999) as a consequence of flow separation. As the flow speed increases (i.e., F approximately equal to 0.5), enhanced vertical displacements will occur both ahead and behind the obstacle, and wake and boundary mixing zones may develop (e.g., Fig. 3). The three-dimensional character of the flow is difficult to present, and so a coplanar view of streamlines is adopted in Figs. 3–5. Significant displacements into and/or out of the respective planes are represented by dashed streamlines. The vertical plane is assumed to be nearly on axis (upper panels); the horizontal plane (lower panels) represents streamlines that originate at approximately 3/4 times the bump height.

Ahead of the bump, the flow nearest the free surface experiences little displacement. Flow near $z = h$ is drawn up and over and then accelerates down the lee side in the beginning of a lee wave. Flow from much below the obstacle height (i.e., $z < 0.8h$), rises slightly during the approach but has insufficient inertia to overcome the buoyancy, and it splits around the lower portion of the bump. Outside a thin convergent boundary layer, one might expect the flow speeds to be slightly accelerated both over and around the bump, and there

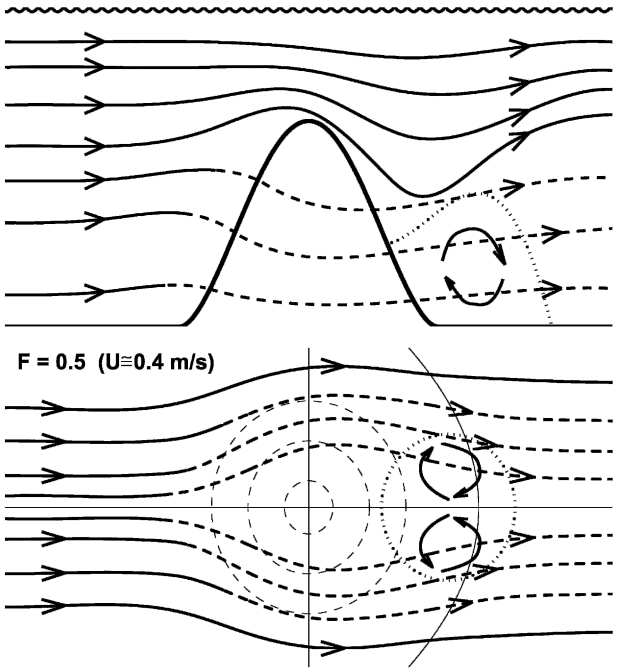

FIG. 3. The idealized stratified flow streamlines over a bump at F approximately equal to 0.5 (based on Hunt and Snyder 1980). (top) The vertical plane, near the center axis of the bump. (bottom) A representative horizontal plane, following streamlines that start at a height of approximately (3/4)h. Displacement of streamlines into and out of the planes is represented by dashed streamlines. Approximate wake and possible mixing zones are enclosed by a dotted line. The arc in the lower panel represents the approximate range of positions occupied by the moored ADCPs.

may be a region of stagnant fluid within an attached wake zone (dotted line).

In a tidal flow, the current direction and magnitude vary over a tidal cycle. Near Victoria, the tides are mixed semidiurnal, with both a *strong ebb* and *strong flood*, followed by a *weak ebb* and *weak flood*. The elliptical nature of tidal currents dictates that the direction (axis) of the currents rotates during the tidal cycle. Our moored ADCPs were at fixed locations on the ebb-lee side of the bump and so lie on a curve, approximately represented by the thin black arc in the lower panels of Figs. 3–5. At times, the moorings will be on the left flank (looking downstream), at other times directly in the wake, and at yet other times on the right flank. As a consequence, by observing numerous tidal cycles, we observe different portions of the wake region behind the bump.

As the flow speed increases and F is approximately equal to 1.0, more of the approaching fluid is forced over the bump, increasing the convergence and accelerating the flow (Fig. 4). The uppermost fluid will be influenced, and the free surface may be altered, both by the introduction of elevations and depressions and through the interactions between surface waves and the accelerated flow. As the converged, accelerated flow passes over the top, the streamlines plunge steeply. The vertically displaced isopycnals will form an internal lee wave (Fig. 4) with a height of Fh (Vosper et al. 1999).

A hydraulic jump may also develop (Fig. 4, upper panel). Hunt and Snyder (1980) make little distinction between regions in which the flow rises sharply and those characterized by a true "hydraulic" jump. Vosper et al. (1999) conduct similar laboratory experiments but employ an acoustic Doppler velocimeter to characterize the turbulent nature of the wake zone. In the classic theory (i.e., Huppert and Miles 1969), a hydraulic jump represents an important region of transition between critical and subcritical flow, corresponding to a region of significant energy dissipation. For our purposes, a region of the flow where "jumps" may occur is likely to have enhanced mixing and turbulence, where kinetic energy is not only dissipated but is also converted to potential energy through the mixing of the stratified fluid.

As the flow speed increases further, so that $F > 1$, additional transitions may develop (Fig. 5). The internal lee wave generated at lower F will no longer be able to buck the flow and will get swept downstream at a rate equal to the difference between the flow speed and the most significant internal wave speed. Approaching streamlines close to the bottom will experience significant vertical excursions, with decreasing horizontal displacements. A supercritical flow passing over the top

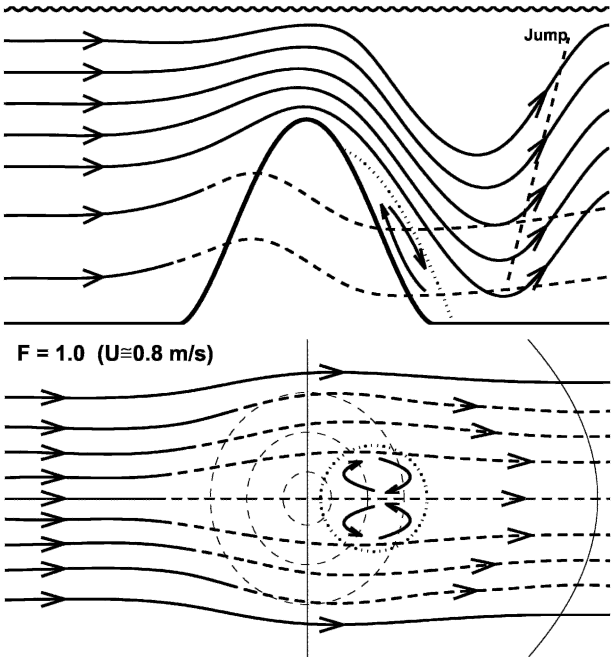

FIG. 4. As in Fig. 3, but for F approximately equal to 1.

and/or over a lee wake may lead to flow separation near the crest and there will be a reduced pressure drop associated with the enlarged wake zone (Fig. 5). Shears within the wake region may be large, further enhancing the likelihood of instabilities and enhanced local turbu-

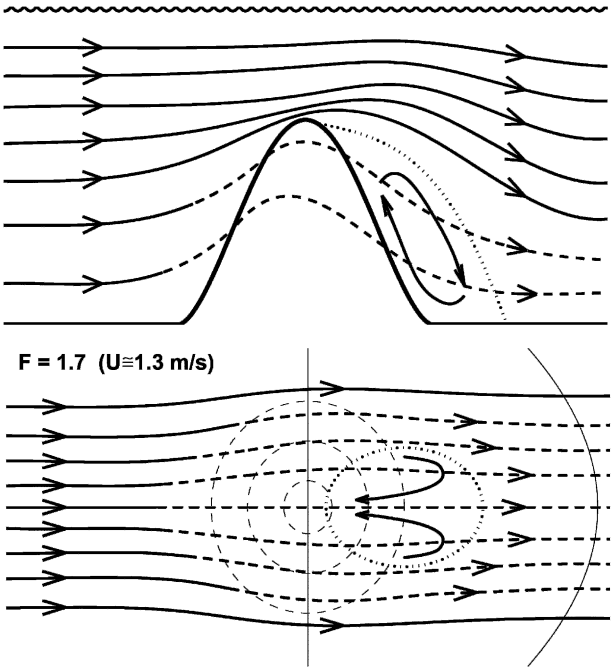

FIG. 5. As in Fig. 3, but for F greater than 1.

lence. Also of note are possible variations in the position and extent of the boundary wake regions over the full range of F, as it first diminishes and then grows with increasing F (Figs. 3–5).

In a time-varying flow (i.e., tides), the decelerating phase may allow conditions to pass back through the critical Froude number regime. During slack and reversing current directions, lee waves may be released and propagate back over or past the obstacle in the opposite direction to the flow that generated them. If, however, the rate of change of flow is too rapid or the frequency of flow variation ω is too high, the flow may never approach a quasi-steady state. In particular, the development of a significant lee wave requires that the flow support conditions near $F \sim 0.7$ for a period comparable to L/U. For our bump, in a semidiurnal tide $\omega L/U \ll 1$, the flow is quasi steady over most of the tidal cycle, and a significant lee wave could develop over an interval as short as 10 min. Further complicating the temporal variability of the flow is the fact that tidal currents rotate during a tidal cycle, altering the location and direction of wakes and wave disturbances.

4. Observations

Our primary tools were two bottom-mounted 300-kHz ADCPs and a vessel-mounted 150-kHz ADCP. The bottom-mounted ADCPs were deployed on the ebb-lee base (Fig. 1, insert), with one (ADCP-West) positioned on what was anticipated to be the central axis of the ebb flow as predicted by regional tidal models (Foreman and Thomson 1997) and the second (ADCP-East) positioned slightly off axis to the southeast (left flank), in the boundary between the wake and the circulation around the bump. Both ADCPs were programmed to sample the full water column (100 m) with 1-m vertical bins, recording 15-ping ensembles every 10 s. The bottom mounts were equipped with gimbals to assist the ADCPs in obtaining a vertical orientation. The ADCPs were deployed from approximately 1100 PST 19 June through 1400 PST 23 June 2002, covering eight complete M_2 tidal periods. Spatial surveys utilizing the shipboard ADCP were conducted during ebb tides along a repeated track that would provide sections over the bump and the bottom-mounted ADCPs. The ship-mounted 150-kHz ADCP was set to record 6-s ensembles with 4-m vertical bins. CTD casts and tow-yo surveys were also conducted throughout the region during this interval, primarily during flood tide, when the moored ADCPs were on the upstream side of the bump.

The measured currents were dominated by mixed semidiurnal tides, with a weak ebb and flood followed by a subsequent stronger ebb and flood (Fig. 6). Superimposed on these tides is a weak mean estuarine circulation driven by river discharge into the inland basins of the Strait of Georgia (primarily the Fraser River) and Puget Sound (primarily the Skagit River). Although subtle variations in the stratification were measured during the 4-day observations, $\overline{N}$ is approximately equal to 1.1×10^{-2} s^{-1} over the upper 80 m (Fig. 7), and therefore to a good approximation $F(t)$ is approxi-

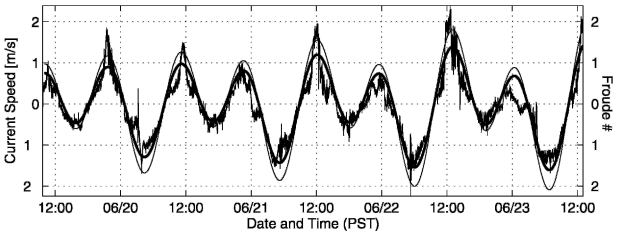

FIG. 6. Currents measured by ADCP-East (fine line) averaged over the height interval 60–70 m, predicted tidal currents U_{tide} northeast of the bump (thick curve; Foreman and Thomson 1997), and the approximate Froude number (thin curve), based on $F = U_{\text{tide}}/0.77$.

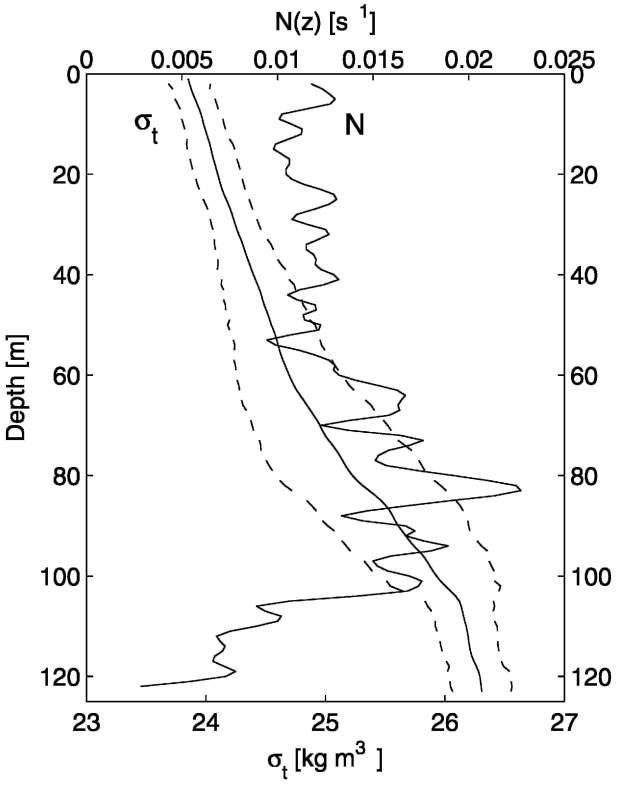

FIG. 7. The average density profile from over 40 CTD casts taken in the region of the bump, with 1-std-dev bounds, and the corresponding $N(z)$ profile.

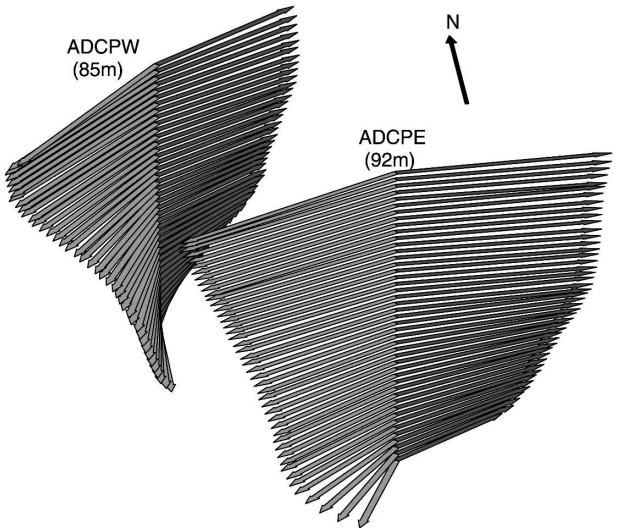

FIG. 8. Hodograph profiles of the principal axes during ebb (toward lower left) and flood (toward upper right) tides. Alternate ADCP bins are shown (i.e., 2-m separation) from a height of 4 m to the highest ADCP bin uncontaminated by surface interference.

mately equal to $U(t)/0.77$ (Fig. 6), where $U(t)$ is the unperturbed upstream tidal speed in meters per second, which we take from the regional barotropic tidal model of Foreman and Thomson (1997).

An analysis of the moored ADCP profiles identified the dominant axes of the flow at each depth, during both flood and ebb. The procedure simply calculates the axis of maximum variance ($U^2 + V^2$) for the recorded time series, including both the tides and mean flow components. Figure 8 shows hodographic profiles of the principal axes during ebb and flood up to a height of approximately 95 m, for both ADCP-W (upper left) and ADCP-E (lower right). From approximately 70-m height to the surface (100 m), the current directions during both ebb and flood are uniform with depth; below the top of the bump, the axes of the flows rotate toward a north–south preference. Ebb tides are directed more toward the southwest, whereas flood tides are directed more toward the northeast.

To identify the more robust flow characteristics that are repeated each tidal cycle, a formal harmonic tidal analysis was conducted to identify the exact tidal phasing. Three complete "tidal days" were fully resolved, based roughly on 2 times the M_2 period. When the upper water column (top 40 m) current vectors are rotated onto an average M_2 axis and averaged over a composite M_2 tidal day (24.63 h), some robust features become evident (Fig. 9), suggesting a high degree of reproducible structure in the flow and the effects generated by the bump. For purposes of discussion, we have identified the phases of the tide as strong flood, followed by weak ebb, weak flood, and strong ebb. Some features of note (Fig. 9) are the following:

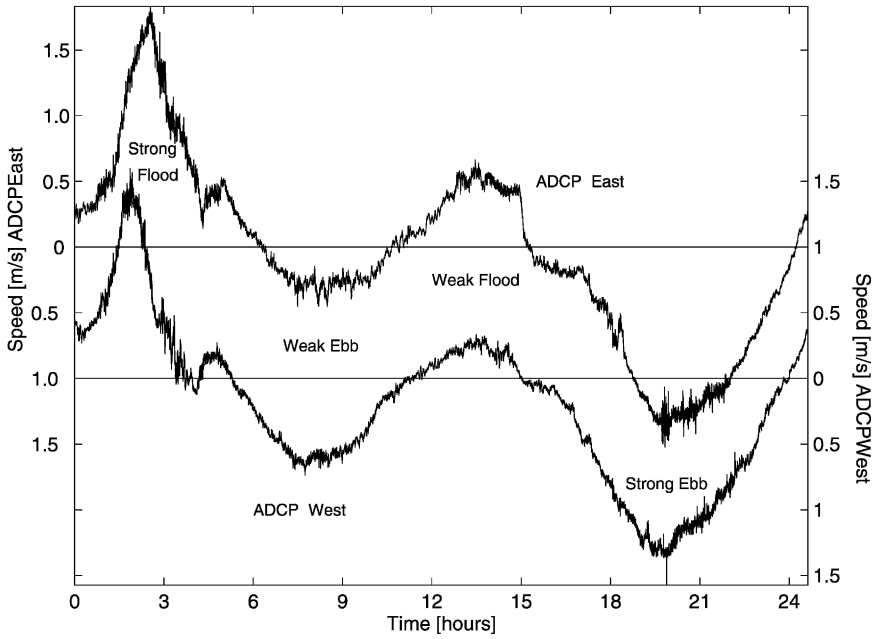

FIG. 9. Tidal phase-averaged flow along the M_2 axis for the ADCP-West and ADCP-East records. The principal-axis components were averaged both temporally over three complete "tidal days" (24.63 h) and vertically over the upper (10 m < depth < 50 m) water column. Time is relative tidal phase.

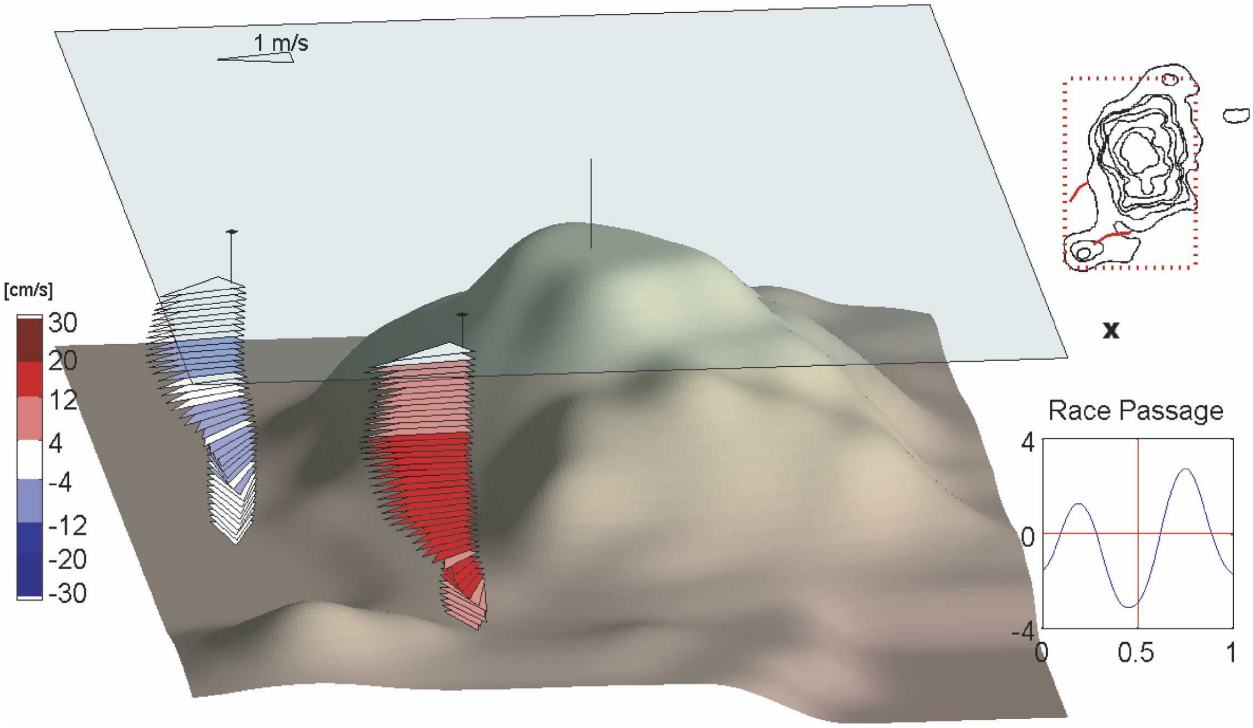

FIG. 10. Hodographic representation of the bump and instantaneous moored ADCP profiles for 0605:54 PST 22 Jun 2002 during a strong ebb. Color coding identifies the vertical velocity (positive up). The upper-right graphic shows the principal axes of the flow and the "camera" location (cross). The vertical red line in the lower-right graphic shows the time relative to tidal currents at Race Rocks tidal station.

1) The strong flood is brief, possibly being delayed or affected by processes occurring upstream at Race Rocks.
2) The transition from strong flood to weak ebb in the West record leads that in the East record by about an hour.
3) The weak ebb is stronger (by 0.25 m s^{-1}) in the West record, whereas the weak flood is stronger in the East record.
4) The strong ebb is similar in phasing and magnitude for both the West and East records.
5) Some higher-frequency signals have survived the vertical and temporal averaging and are identifiable in both records (e.g., the wavelike feature near hour 5 and fluctuations occurring at hour 20; Fig. 9).

To investigate some of these features further, animated three-dimensional hodographs were employed. Viewing the flow in an animated presentation allowed for many subtle characteristics to be identified.

5. Analysis and discussion

The nature of the flow over an isolated bump is inherently four-dimensional. Display and analysis of the ADCP profile time series were aided by projecting successive hodographs of the velocity vectors onto an approximate three-dimensional representation of the bump (Fig. 10). Vector arrowheads are used to display the horizontal U and V velocity data, and color is used to indicate vertical velocities (W). Animating successive images further enhanced our ability to visualize the temporal flow characteristics resolved by the two moored ADCPs. Over a tidal cycle, the flows represented a wide range of Froude number regimes, corresponding to flows that were more horizontal (F approximately equal to 0.2), through critical conditions (F approximately equal to 1), to supercritical flow (F greater than 1). In addition, the rotary nature of the tides resulted in a variety of "attack" angles. Because the moorings were fixed relative to the bump, these varied current directions allow us to realize various regions of the wake behind the bump (i.e., Figs. 3–5).

Through patient viewing of the animated hodographs (over 35 000 individual profiles/frames), many features that were repeated during common tidal phases and several relevant three-dimensional structures were identified. The most dominant of these features include

- repeated lee-wave formation and separation during the developing strong ebb,

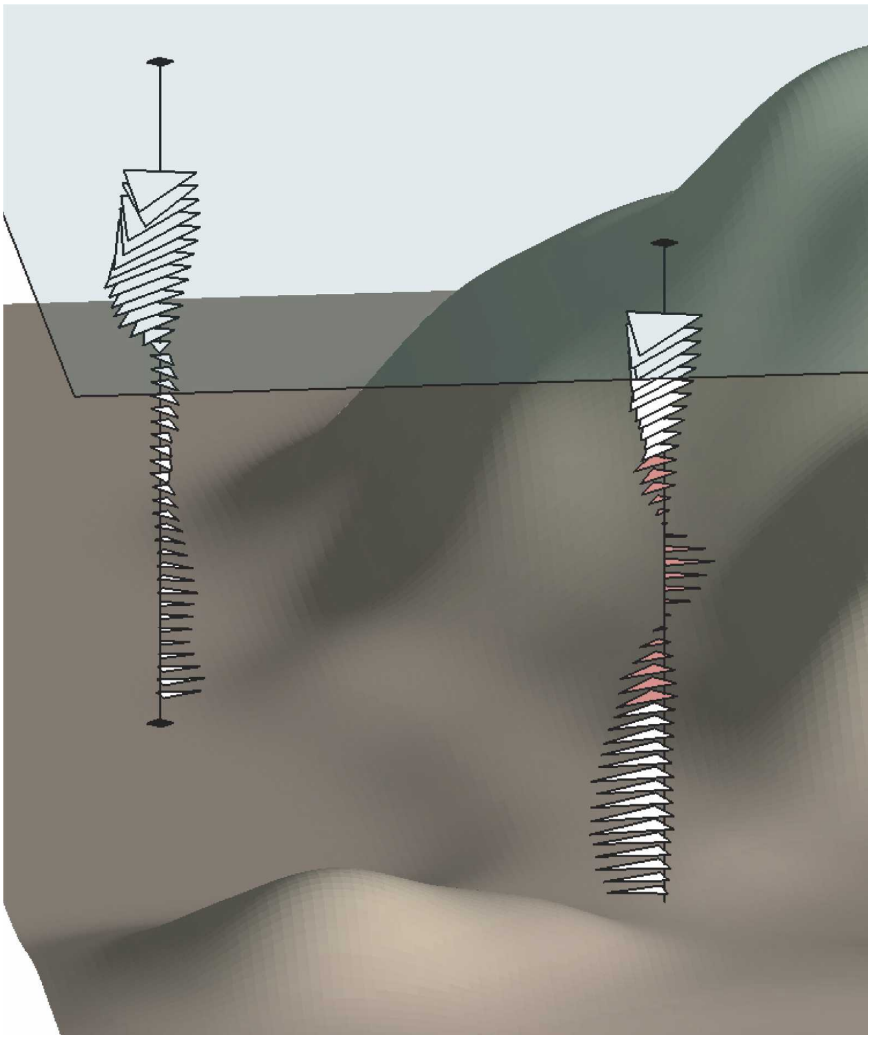

FIG. 11. Hodographic representation of 1-min-averaged ADCP profiles for 1715:04 PST 20 Jun 2002 during a weak ebb (tidal-phase hour 8). Color coding identifies the vertical velocity (W), as in Fig. 10.

- complex shears, both horizontally and vertically, throughout all phases of the tide, and
- persistent rotary tendencies in the bottom boundary layer at consistent phases of the tide.

In light of the preconceptions of how a stratified flow might interact with an obstacle (Figs. 3–5), we will examine the more interesting and robust features captured in the observations corresponding to subcritical, critical, and supercritical conditions.

a. Subcritical flow

During the weak ebb, the upper water column current directions were persistently aligned in the north–south direction (Fig. 11). In this orientation, the ADCP-West mooring is aligned more with the right flank of the bump (when viewed from upstream), whereas the ADCP-East is directly behind the bump. The Froude number (Fig. 6) peaks at F approximately equal to 0.7, corresponding to near-critical conditions similar perhaps to those represented in Fig. 3. Uniform currents were seen in the upper portions of the water column, corresponding to heights above the bump (Fig. 10). Below the top of the bump, the currents at ADCP-West were persistently weak and often veered inward, toward the bump, possibly toward a region of low pressure in the wake (Fig. 3). The deeper currents at ADCP-East were more varied in time, with strong rotary shears and occasional vertical velocities, consistent with a deep fluctuating wake region. Except right at the bottom, the lower portion of the ADCP-East profile consistently veers to the west (Fig. 11), suggesting that

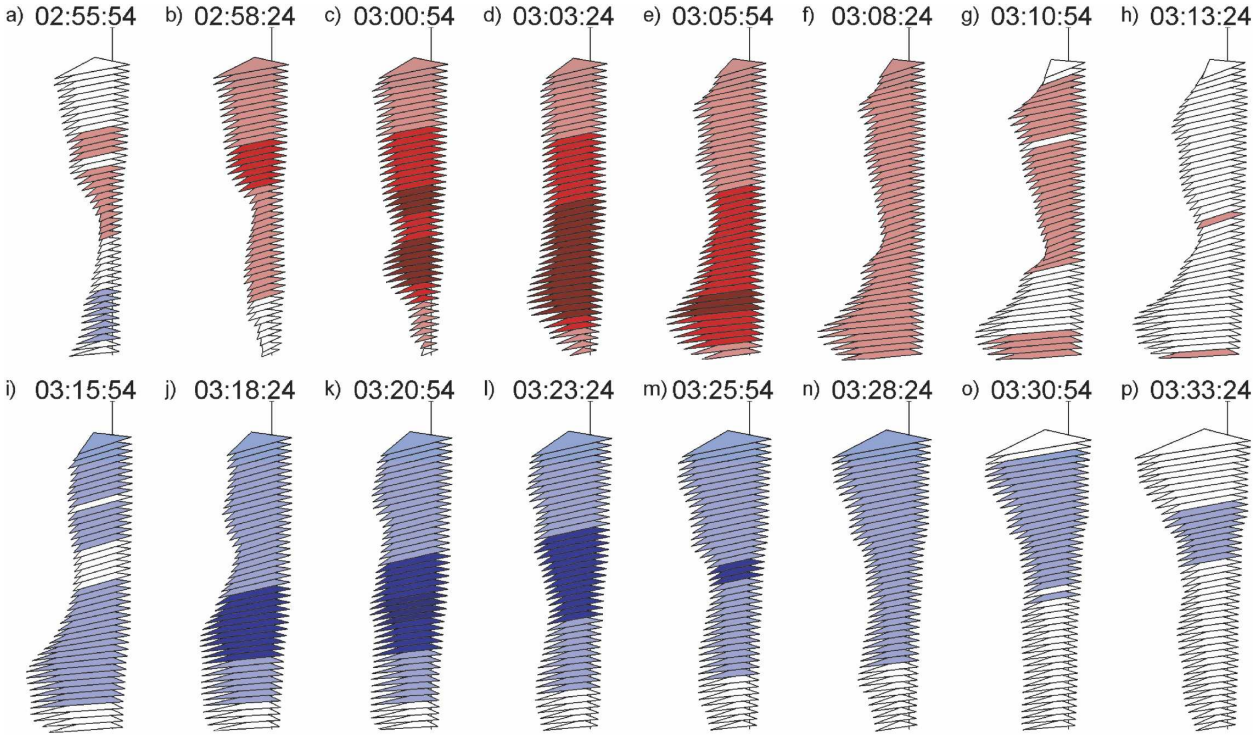

FIG. 12. Hodographic representation of the ADCP-East record, showing successive (from upper left to lower right) 2.5-min-averaged profiles of three-dimensional velocity, where vertical velocities are color coded (red upward; blue downward) as in Fig. 10, from 0255 to 0334 PST 21 Jun 2002, corresponding approximately to tidal-phase hour 18 (Fig. 9).

it is on the eastern side of the wake, with an inflow similar to that seen at ADCP-West. Consistent with Fig. 3, the wake region is both wide (affecting both moorings) and deep (comparable to the height of the bump). Although there are strong shears realized in both moorings, there is no indication of either hydraulic jumps or lee waves, although at these speeds, any such disturbance would be confined to the region between the moorings and the bump. Last, contrary to the low-F findings of Vosper et al. (1999), examination of the time series shows no evidence of coherent eddy shedding behind the bump.

b. Critical flow and lee waves

During the development of each strong ebb (e.g., tidal-phase hours 17–21; Fig. 9), several features consistent with the anticipated effects of an obstacle at subcritical, critical, and supercritical flows conditions were realized. With near-surface currents in the 0.4 m s^{-1} range, corresponding to F of approximately 0.6, currents below the height of the bump at both moorings turn inward as in the weak ebb (e.g., Fig. 11). As each strong ebb continued to developed (i.e., hour 18; Fig. 9) and the Froude number approached 1, a lee wave was repeatedly realized in the ADCP-East record, directly downstream from the bump. Shown in Fig. 12 are progressive 2.5-min-average hodograph vectors for the ADCP-East record corresponding to approximately tidal-phase hour 18 in Fig. 9. The vectors reveal a progression of strong upward vertical velocities (red) from the upper water column to the bottom (left to right across the top panels in Fig. 12), followed by a progression of strong downward vertical velocities (blue) from the bottom to the top (left to right across the bottom panels in Fig. 12). Corresponding closely to the maximum vertical velocities are strong horizontal velocities. This striking feature can also be viewed as a progressive time series of the individual velocity components and acoustic backscatter (Fig. 13). Although only 500 m to the northwest, ADCP-West did not detect this evolving lee wave. Flows there, although highly sheared, were consistently more horizontal in nature.

Our interpretation of this lee wave as revealed by the ADCP-East time series is as follows: While the strong ebb tide develops, the flow over the bump approaches critical conditions and a lee wave develops immediately behind the bump. Our moorings, however, are slightly downstream of this lee-wave development region, which lies between ADCP-East and the crest of the bump (Figs. 3 and 4). As the current increases and the

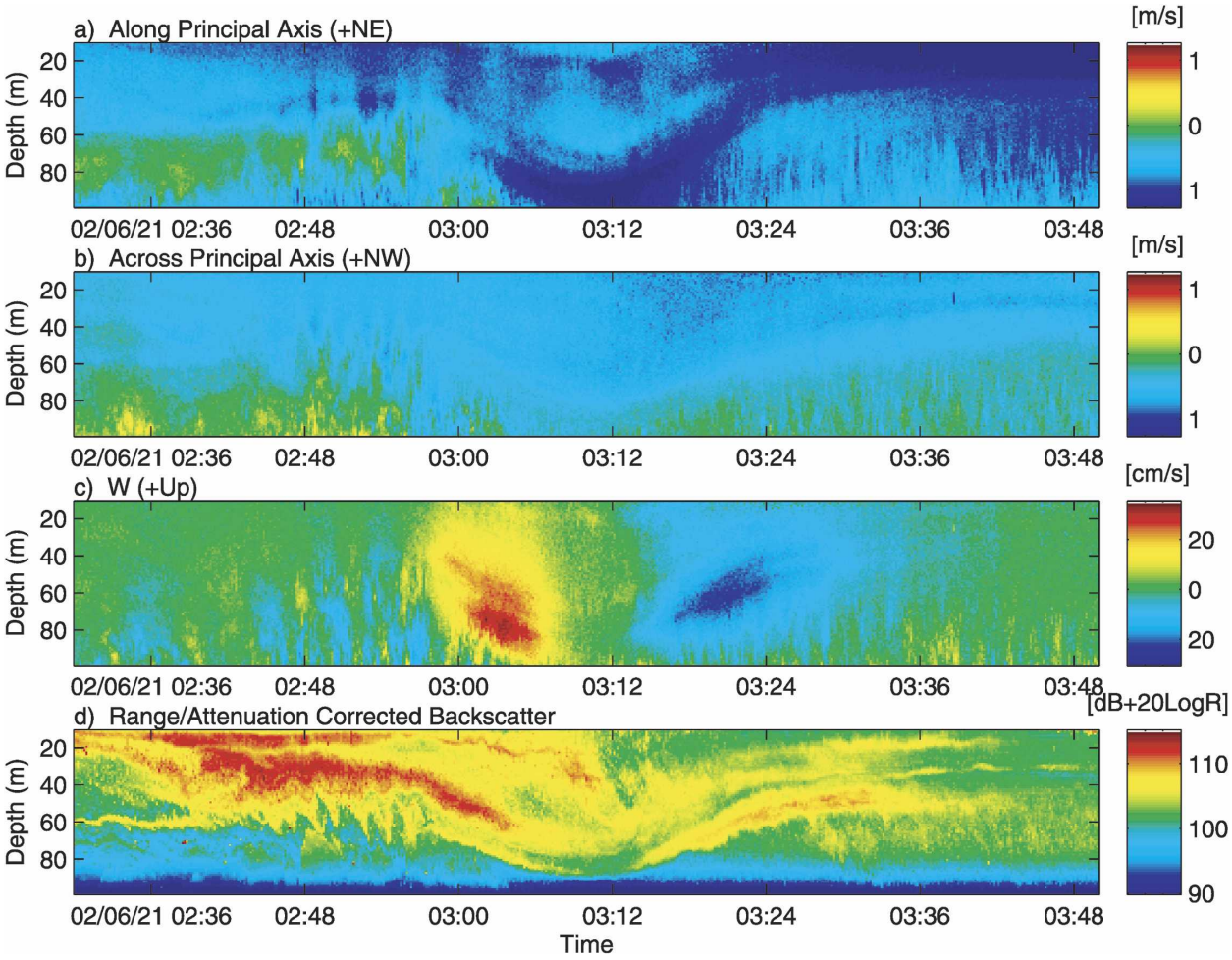

FIG. 13. Time–depth contours of instantaneous (a) along-axis velocity (m s^{-1}), (b) cross-axis velocity (m s^{-1}), (c) vertical velocity (cm s^{-1}), and (d) acoustic backscatter (dB) during a developing strong ebb flow (ADCP-East).

flow over the bump becomes supercritical, the lee wave moves away from the bump crest and is advected over our ADCP-East mooring (Fig. 14). In this case, the ADCP first detects the tail of the lee wave, with strong upward velocities in the upper portion of the water column (0303 PST; Figs. 12 and 13). As the lee wave continues to get advected through the acoustic beams of the ADCP, the upward vertical velocities progress deeper in the water column until the base of the wave passes directly over the ADCP (0311 PST; Figs. 12 and 13). At this point, the flow is nearly entirely horizontal. The horizontal currents in this "jet" are 1.5 m s^{-1}. As the strong ebb builds further, the lee wave continues to be advected downstream of the bump, and the plunging edge of the wave passes over the ADCP, with downward velocities that progress from bottom to top (Figs. 12 and 13). The advection of a lee wave over ADCP-East was realized during the early development of three of the four strong ebb tides (near tidal-phase hour 18; Fig. 9), suggesting a robust interaction between the tidal currents and the bump (Fig. 14).

If the flow over the bump is near critical, then one might expect a hydraulic jump on the trailing edge of the lee wave (Figs. 4 and 5) as evident in the high-frequency backscatter images of Farmer and Armi (1999). Acoustic backscatter (Fig. 13d) intensity suggests that prior to the arrival of the lee wave over the mooring, the flow is highly turbulent with intense backscatter, accompanied by periodic regions of entrainment (i.e., Figure 13d; 0250 PST). The ADCPs used were Janus configurations, with four oblique transducer faces angled 20° from the vertical axis. The fluctuating component of the individual beam velocities (Fig. 15) reveals highly coherent "billows" (between 0248 and 0300 PST), although a formal Reynolds stress calculation following Lu and Lueck (1999) did not produce meaningful stresses. These turbulent-like structures have vertical scales of 20–30 m and temporal durations

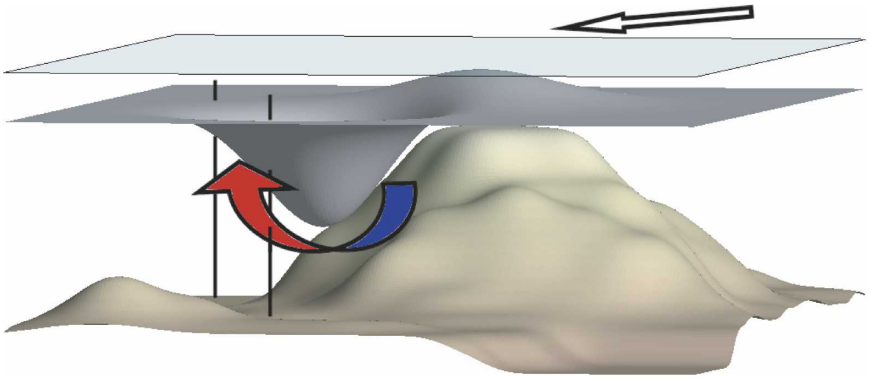

FIG. 14. Artistic interpretation of the strong ebb lee wave as realized by the ADCP-East mooring (right vertical black line). Projected over the bump is a material surface (e.g., isopycnal surface), showing how the flow first accelerates over the bump, rising and then falling into the three-dimensional lee wave in the wake.

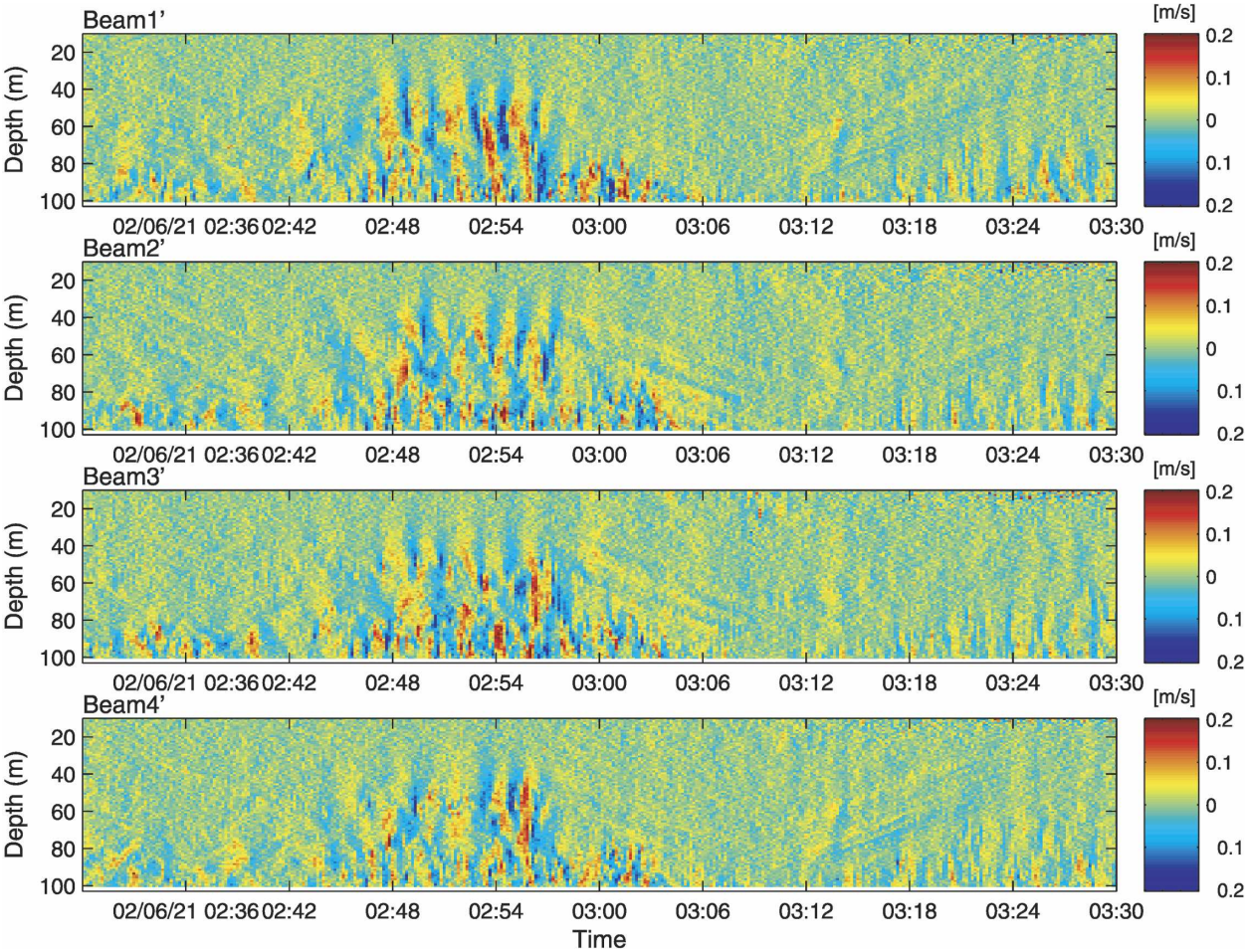

FIG. 15. High-pass-filtered ADCP-East individual beam velocities for 0230–0330 PST 21 Jun 2002. Highly coherent billows are detected in the individual beam velocities just prior to the arrival of the lee wave at 0300 PST.

of 1–2 min (too steep or brief to be internal waves). There is a hint of beam 1 leading beams 2 and 4 by 40–60 s, which is consistent with the beam alignment (Fig. 16), the beam separation with height, and advection with U of approximately 0.5 m s^{-1}. Immediately after the occurrence of these billows (i.e., at 0305 PST; Fig. 15), the beam velocity fluctuations are negligible, corresponding to the passage of the lee wave.

As part of the shipboard ADCP survey work undertaken during each ebb tide, on 21 June a transect directly over the ADCP-East mooring coincided with the passage of the lee wave shown in Figs. 12 and 13. Figure 17a shows a portion of the ship track, starting at the red dot, including two passages over the bump, first from south to north (into the ebb tide), followed by a transect from northeast to southwest (with the ebb tide). Figure 17b is a section of vertical velocities as measured by the ship-mounted 150-kHz ADCP along this ship track. While passing over the ADCP-East location at 0310 PST 21 June, the lee wave is identified by the upward (red) and downward (blue) velocities. Vertical velocities of order 0.3 m s^{-1} were revealed by both the ship and moored ADCPs at 0310 PST 21 June 2002. Upon the return transect slightly to the west, only part of the lee wave wake is crossed (0348 PST), catching a region of weaker downward velocities of order 0.2 m s^{-1} and slight upward velocities of only 0.15 m s^{-1}. Because the bump is three-dimensional, so is the lee wave generated in its wake (Fig. 14). Based on both the ship and moored ADCP records, the width of the lee wave is estimated to be comparable to the width of the bump (about 400 m), whereas the ship survey (Fig. 17b) alone suggests a longitudinal scale of about 200 m. With a wave height of 50 m, the isopycnal slopes are as steep as 1/4.

Lee waves were consistently observed during the development of each strong ebb tide. Current speeds at the moorings and from tidal models (Foreman and Thomson 1997) would suggest that the lee wave was generated while the Froude number approached 1 (Fig. 6). ADCP-West, which was not directly in the wake during the development of the strong ebb, measured slightly higher (by about 0.2 m s^{-1}) current speeds than at ADCP-East (e.g., hour 17; Figure 9), possibly indicating that the currents at ADCP-East were "delayed" by the development of the lee wave. Once the lee wave had advected over ADCP-East, the current speeds rapidly increased (i.e., hour 19; Fig. 9).

c. Supercritical flows

In the later stages of the strong ebb, persistent features were evident that are consistent with the supercritical structures of Fig. 5. The hodographs in Figs. 10 and 18, corresponding roughly with peak ebb tide, show strong (about 1.5 m s^{-1}) currents in the upper water column at both moorings, significant left-turning bias toward the bottom, and complex vertical velocity structures. In the ADCP-East hodograph for 0605:54 PST 22 June (Fig. 10), the entire water column registers upward velocities of greater than 10 cm s^{-1}. Although the anticlockwise shear is consistent with an Ekman boundary layer, the veering of the currents near the bottom might be a consequence of steering by small-scale topographic features. A similar "left hand" bias is also seen during the flood tide (not shown). It is possible that the anticlockwise shear near the bottom during both ebb and flood is an effect of the Coriolis force (Soulsby 1990), even though there is little time to establish a normal Ekman layer.

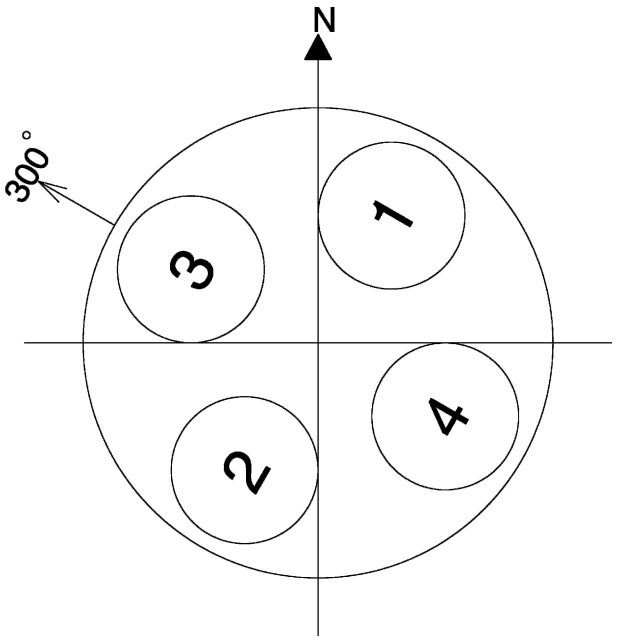

FIG. 16. The moored ADCPs had four transducers arranged in a Janus configuration. The alignment of the ADCP-East is shown with respect to true north, with a compass heading of 280° magnetic.

During the supercritical strong ebbs (e.g., Fig. 18; tidal-phase hour 20, Fig. 9), there are persistent shear patterns. At ADCP-West (left profile, Fig. 18), the currents in the upper water column, from approximately one-half of the bump height upward, are uniform. At approximately 40-m height there are slight downward vertical velocities and a 60° shift toward the left (counterclockwise). Currents in this deep boundary layer are still strong (about 1 m s^{-1}). At ADCP-East (right profile, Fig. 18), there is moderate shear in the upper water column (60–70-m height), upward vertical velocities below 60 m, and a thin (15 m) bottom boundary layer,

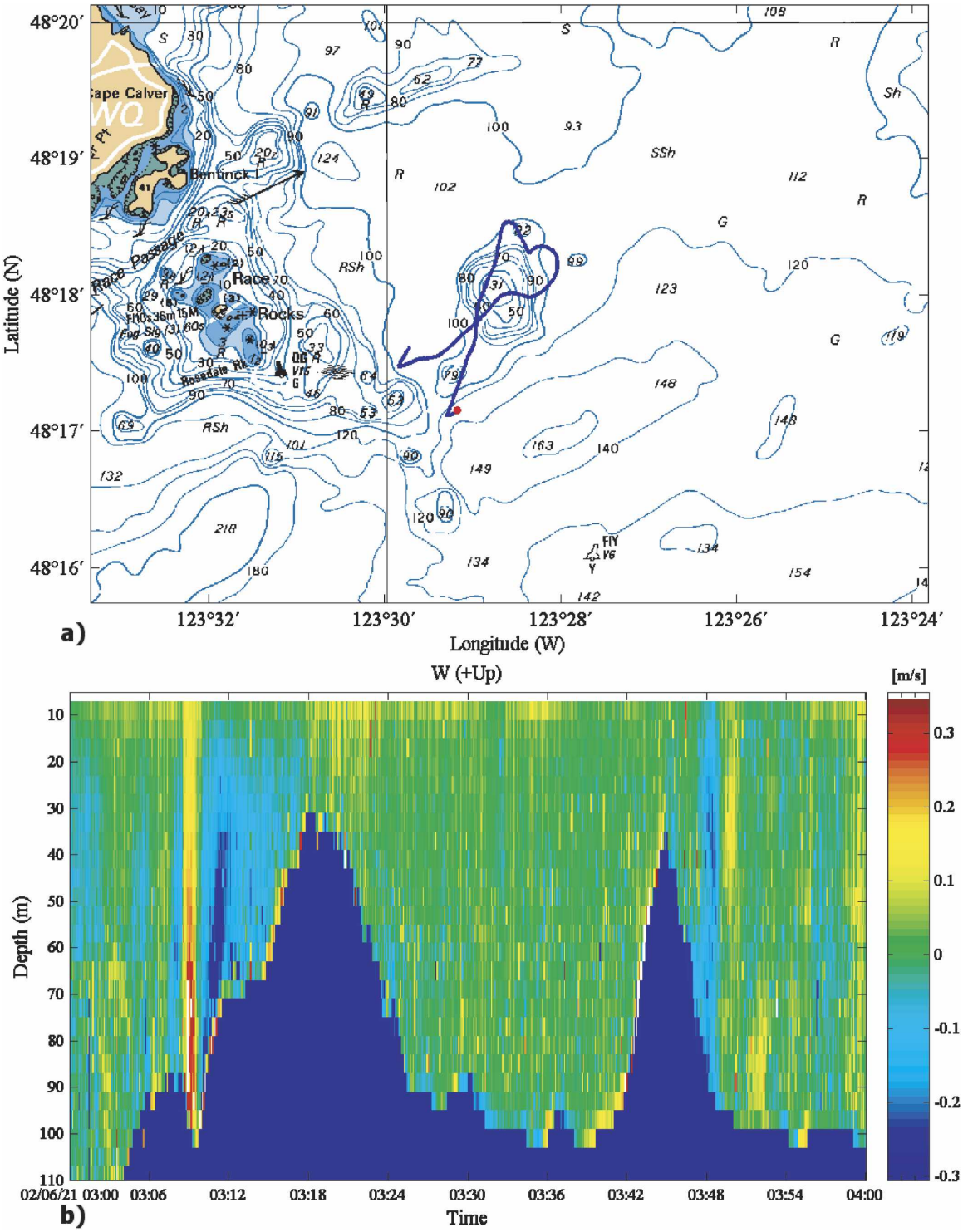

FIG. 17. (a) Ship-track section during the strong ebb tide shipboard ADCP survey early 21 Jun 2002. This portion of the continuous record starts at the red dot. The ship speed was approximately 4 kt (~2 m s^{-1}). (b) The ship-mounted 150-kHz ADCP measured vertical velocities along this track, revealing the same lee wave shown in Fig. 13.

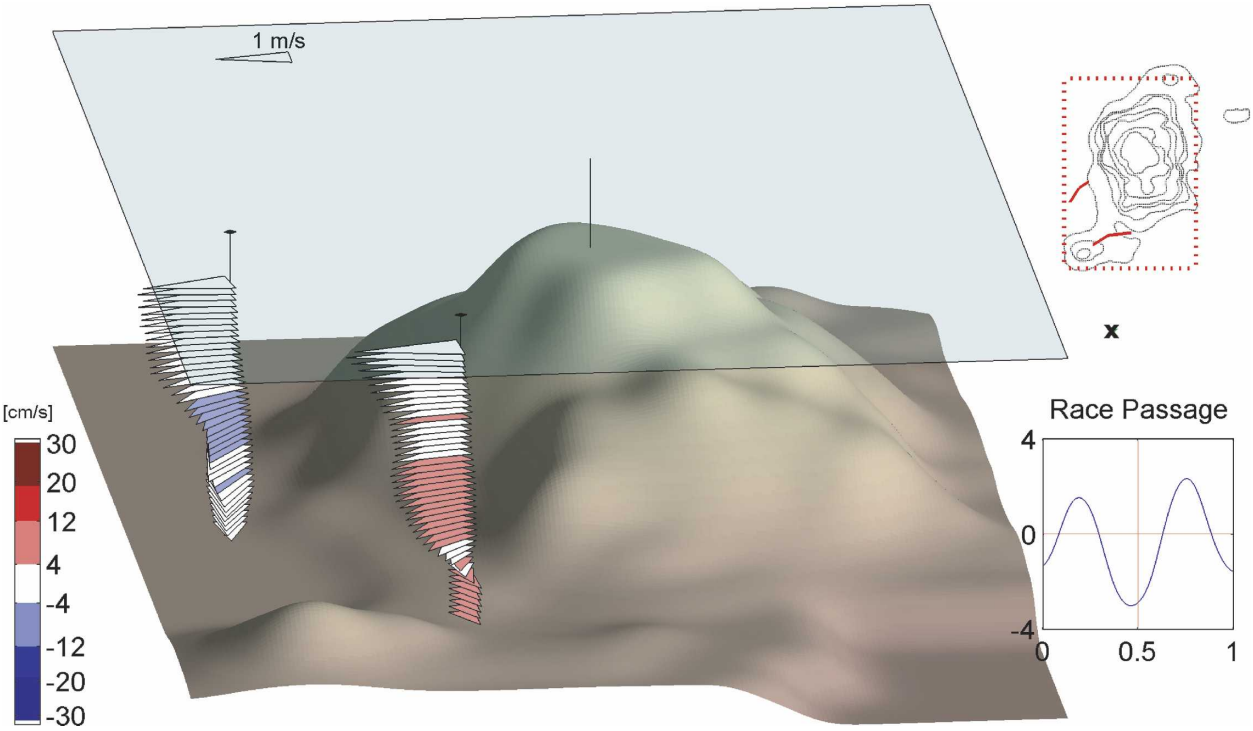

FIG. 18. Hodographic snapshot during the strong ebb at 0500 PST 21 Jun 2002.

where currents veer uniformly to the left. These repeated shear structures are not consistent with the supercritical features sketched in Fig. 5, because the axis of the flow would suggest the moorings are now located on the left flank of the bump and yet both boundary flows are outward, away from the axis of the obstacle.

Despite the recurring detection of the lee wave during the developing strong ebb, we did not observe the return passage of the lee wave as the ebb slackened, although this phenomenon is common in 2D flows (Cummins et al. 2003). Our measurements suggest that the lee wave is highly three-dimensional, and it could easily have passed by both our fixed moorings and periodic ship surveys during its presumed return passage toward the northeast. A future study might be to track the lee wave from formation and separation, through the slackening tide, when it could propagate back over or past the bump.

6. Conclusions

Stratified flows over three-dimensional obstacles are common in both the atmosphere and ocean. Alterations to the flow are both local and, through the generation of internal waves, may influence the environment remotely, far from the topographic feature. Observations of the tidal currents near Victoria, British Columbia, have allowed us to study interactions between a stratified flow and an isolated bump. Many of the three-dimensional flow structures reported by Hunt and Snyder (1980) and Smith (1989) were observed in the two moored ADCP records and ship-based ADCP surveys. Variability of the tidal current direction adds a level of complexity to the interpretation, because the mooring locations sample different regions of the flow during different phases of the tide. Many key features were identified. Some of these features were in agreement with expectations:

- Tidal currents over the bump are quasi steady and allow coherent structures to develop.
- During the weak ebb and low-F flows, a larger wake exists behind the bump and flow on the lee side is at times observed to converge from the sides and/or flow back toward the bump.
- At near-critical Froude number (F approximately equal to 0.7), a large lee wave develops in the wake. The ship-mounted ADCP realization of the three-dimensional lee wave suggests it has a horizontal wavelength of 200 m and isopycnal slopes of about 0.25.
- In the lee of the lee wave, the flow is turbulent, as expected within a hydraulic jump.
- The lee wave is highly three-dimensional and is only seen in one of the moored ADCP records.

- As the flow becomes supercritical ($F \geq 1$), the lee wave is advected downstream of the bump (separation), getting swept over the ADCP-East mooring location.
- The generation of lee waves and wakes is highly repeatable over successive tidal cycles for a wide range of Froude numbers.

Some of the flow characteristics measured by the ADCPs were unexpected and are not directly consistent with the symmetrical obstacles or theory utilized to construct the interactions simplified in Figs. 3–5:

- Midwater column shear during both ebb and flood is asymmetrical. This condition could be due to the fact that the bump is neither smooth nor ideal in shape, and even small irregularities might introduce disturbances that cause asymmetries in the flow.
- During the slackening ebb tide, the "released" lee wave was not observed, possibly a consequence of its limited spatial size and our restricted observations. Tracking the lee wave during development, separation, and release might be an interesting exercise for a future experiment.
- A left-hand shear in the bottom boundary layer was evident during all strong ebb tides and often during the flood tides. Irregularities in the shape of the bump could easily introduce small pressure disturbances that might cause the boundary layer currents to veer leftward during the ebb tides, although Coriolis effects may also be important.

To quantify the drag induced by isolated obstacles such as our bump, one would need to measure the barotropic and baroclinic pressure disturbances, as well as the turbulence within the bottom boundary layer and attached wake regions. Although we have little evidence that our bump generated significant barotropic wakes such as the eddies realized by Edwards et al. (2004), the observed lee wave clearly represents a significant extraction of momentum and energy by the generation of internal waves. Parameterization of this drag may be accounted for by simply increasing the local drag coefficient. The linear theory of Miles (1969), Phillips (1984), and Smith (1989) indicates that the internal pressure disturbances and energy loss to internal wave generation can be represented by an internal drag coefficient given by

$$C_D = \frac{\pi}{2F}, \tag{3}$$

where F is the topographic Froude number [Eq. (2)]. For our flows, this drag coefficient would peak near unity. Equation (3) implies that the drag coefficient decreases as the Froude number increases, although the effective drag on the flow, $D = (1/2)C_D\rho U^2 A$, where A is the area, would continue to increase as the tidal current grows. Such a parameterization accounts for the local extraction of momentum but does not address the equally interesting and important remote dissipation of the energy (Althaus et al. 2003). We have little direct evidence of the propagation characteristics of the lee wave, although backscatter satellite imagery of the region consistently shows internal wave packets radiating tens of kilometers away from the Race Rocks area. Tracking and following the internal lee wave would be the next important study, to see how far it travels before interacting with either other waves, shear layers, or the bottom.

Acknowledgments. We thank the officers and crew of the CCGS *Vector* for their professional execution of our cruise plan. Fruitful discussions with Parker MacCready and Jim Moum were most helpful, and we greatly appreciate the valuable comments of two anonymous reviewers. The authors were supported by the U.S. Office of Naval Research and the Natural Sciences and Engineering Research Council of Canada.

REFERENCES

Althaus, A., E. Kunze, and T. Sanford, 2003: Internal tide radiation from Mendocino Escarpment. *J. Phys. Oceanogr.,* **33,** 1510–1527.

Baines, P. G., 1995: *Topographic Effects in Stratified Flows.* Cambridge University Press, 482 pp.

Belcher, S. E., and J. C. R. Hunt, 1998: Turbulent air flow over hills and waves. *Annu. Rev. Fluid Mech.,* **30,** 507–538.

Cummins, P. F., S. Vagle, L. Armi, and D. M. Farmer, 2003: Stratified flow over topography: Upstream influence and generation of nonlinear internal waves. *Proc. Roy. Soc. London,* **459A,** 1467–1487.

Edwards, K. A., P. MacCready, J. N. Moum, G. Pawlak, J. M. Klymak, and A. Perlin, 2004: Form drag and mixing due to tidal flow past a sharp point. *J. Phys. Oceanogr.,* **34,** 1297–1312.

Farmer, D. M. and L. Armi, 1999: Stratified flow over topography: The role of small-scale entrainment and mixing in flow establishment. *Proc. Roy. Soc. London,* **455A,** 3221–3258.

Foreman, M. G., and R. E. Thomson, 1997: Three-dimensional model simulations of tides and buoyancy currents along the west coast of Vancouver Island. *J. Phys. Oceanogr.,* **27,** 1300–1325.

Hanazaki, H., 1994: On the three-dimensional internal waves excited by topography in the flow of a stratified fluid. *J. Fluid Mech.,* **263,** 293–318.

Hunt, J. C. R., and W. H. Snyder, 1980: Experiments on stably and neutrally stratified flow over a model three-dimensional hill. *J. Fluid Mech.,* **96,** 671–704.

Huppert, H. E., and J. W. Miles, 1969: Lee waves in a stratified

flow. Part 3: Semi-elliptical obstacle. *J. Fluid Mech.,* **55,** 481–496.

Klymak, J. M., and M. C. Gregg, 2001: The three-dimensional nature of flow near a sill. *J. Geophys. Res.,* **106,** 22 295–22 311.

Kunze, E., and J. M. Toole, 1997: Tidally driven vorticity, diurnal shear, and turbulence atop Fieberling Seamount. *J. Phys. Oceanogr.,* **27,** 2663–2693.

Lamb, K. G., 1994: Numerical experiments of internal wave generation by a strong tidal flow across a finite amplitude bank edge. *J. Geophys. Res.,* **99,** 843–864.

Lu, Y., and R. G. Lueck, 1999: Using a broadband ADCP in a tidal channel. Part II: Turbulence. *J. Atmos. Oceanic Technol.,* **16,** 1568–1579.

Lueck, R. G., and T. D. Mudge, 1997: Topographically induced mixing around a shallow seamount. *Science,* **276,** 1831–1833.

Miles, J. W., 1969: Waves and wave drag in stratified flows. *Proc. 12th Inst. Congress of Applied Mechanics,* M. Hetenyi and W. G. Vincenti, Eds., Spinger-Verlag, 52–76.

Nash, J. D., and J. N. Moum, 2001: Internal hydraulic flows on the continental shelf: High drag states over a small bank. *J. Geophys. Res.,* **106,** 4593–4612.

Phillips, D., 1984: Analytic surface pressure and drag for linear hydrostatic flow over three-dimensional elliptic mountains. *J. Atmos. Sci.,* **41,** 1073–1084.

Rudnick, D., and Coauthors, 2003: From tides to mixing along the Hawaiian Ridge. *Science,* **301,** 355–357.

Smith, R. B., 1978: A measurement of mountain drag. *J. Atmos. Sci.,* **35,** 1644–1654.

——, 1980: Linear theory of stratified hydrostatic flow past an isolated mountain. *Tellus,* **32,** 348–364.

——, 1989: Hydrostatic airflow over mountains. *Advances in Geophysics,* Vol. 31, Academic Press, 1–41.

Soulsby, R., 1990: Tidal-current boundary layers. *The Sea,* B. L. Mehaute and D. M. Hanes, Eds., Ocean Engineering Science, Vol. 9, John Wiley and Sons, 523–566.

St. Laurent, L., and C. Garrett, 2002: The role of internal tides in mixing the deep ocean. *J. Phys. Oceanogr.,* **32,** 2882–2899.

Vosper, S. B., I. P. Castro, W. H. Snyder, and S. Mobbs, 1999: Experimental studies of strongly stratified flow past three-dimensional orography. *J. Fluid Mech.,* **390,** 223–249.

Wolanski, E., T. Asaeda, A. Tanaka, and E. Deleersnijder, 1996: Three-dimensional island wakes in the field, laboratory experiments and numerical models. *Cont. Shelf Res.,* **16,** 1437–1452.